

Polydispersity stabilizes Biaxial Nematic Liquid Crystals

S. Belli¹, A. Patti², M. Dijkstra³, and R. van Roij¹

¹*Institute for Theoretical Physics, Utrecht University,
Leuvenlaan 4, 3584 CE Utrecht, The Netherlands*

²*Instituto de Química Avanzada de Cataluña, CSIC, C/ Jordi Girona 18-26, 08034 Barcelona, Spain*

³*Soft Condensed Matter Group, Debye Institute for NanoMaterials Science,
Utrecht University, Princetonplein 5, 3584 CC Utrecht, The Netherlands*

Inspired by the intriguing observations of a remarkably stable biaxial nematic phase [E.v.d. Pol *et al.*, Phys. Rev. Lett. **103**, 258301 (2009)], we investigate the effect of size polydispersity on the phase behavior of a suspension of boardlike particles. By means of Onsager theory within the restricted orientation (Zwanzig) model we show that polydispersity induces a novel topology in the phase diagram, opening a huge stable biaxiality regime in between uniaxial nematic and smectic states. Besides explaining the experimental results, we suggest system properties that may allow for stabilization of biaxial nematic thermotropic liquid crystals.

PACS numbers: 82.70.Dd, 61.30.Cz, 61.30.St, 64.70.M-

Since its first prediction back in the early 1970s [1–3], the biaxial nematic (N_B) phase has strongly attracted the interest of the liquid crystal (LC) community [4]. In contrast to the more common uniaxial nematic (N_U) phase, where cylindrical symmetry with respect to the nematic director determines optical uniaxiality, the N_B phase is characterized by an orientational order along three directors and consequently by the existence of *two* distinct optical axes. The prospect of inducing orientational ordering along three directions, while maintaining a nematic fluid-like mechanical behavior [5], renders biaxial nematics preeminent candidates for next generation LC-based displays [6]. Although experimental evidences of stable N_B phases were reported already 30 years ago in lyotropic LCs [7], in thermotropics this result was achieved in systems of bent-core molecules only a few years ago [8]. Actually, when trying to experimentally reproduce an N_B phase, one often encounters practical problems related to its unambiguous identification [4] and to the presence of competing thermodynamic structures [9–11]. Stabilizing N_B states is therefore an open, challenging scientific problem with huge potential applications. Motivated by the exciting and to some extent surprising results of a recent experiment on a colloidal suspension [12], we use here a mean-field theory to investigate the role played by size polydispersity on the stability of biaxial nematics in systems of boardlike particles. We show that a difference in the particles volume gives rise to a new topology in the phase diagram of a binary mixture, where the appearance of two Landau tetracritical points determines a wider region of N_B stability. This feature is shown to hold also for a larger number of components. Our model, which offers an interpretation key for the results of Ref. [12], can also furnish a new way to look for biaxiality in thermotropic LCs.

At low density in lyotropics, and at high temperature in thermotropics, the N_B phase appears as a crossover regime in between “rod-like” and “plate-like” behavior [2]. In fact, one can distinguish between the N_U phase developed by rods, in which particles align the longest

axis along a common direction (nematic uniaxial *prolate*, N_+), and that developed by plates, in which particles align the shortest axis (nematic uniaxial *oblate*, N_-). A natural candidate system for developing an N_B phase is a binary mixture of rods and plates [13]; however, in most cases a demixing transition into two uniaxial nematic phases, i.e. N_+ and N_- , prevents its stabilization [10, 11]. Alternatively, a stable N_B state is expected in a system of particles with cuboid (i.e. rectangular parallelepiped) shape defined by the lengths of the principal axes $L \geq W \geq T$, as depicted in Fig. 1(a) [3]. In this case, it is convenient to introduce a *shape parameter* ν , defined by

$$\nu = \frac{L}{W} - \frac{W}{T}. \quad (1)$$

By increasing the packing fraction and disregarding the possible stability of inhomogeneous phases, a system of cuboids undergoes an $I \rightarrow N_+ \rightarrow N_B$ sequence of phases if $\nu > 0$, whereas an $I \rightarrow N_- \rightarrow N_B$ sequence is found if

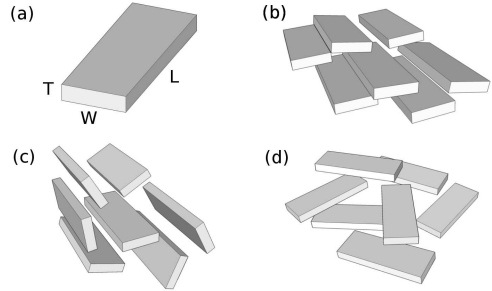


FIG. 1. (a) Cuboidal particle with dimensions $L \times W \times T$. (b) Schematic representation of a system of freely rotating cuboids in the biaxial nematic phase N_B , (c) the uniaxial nematic prolate N_+ and (d) the uniaxial nematic oblate N_- . In this work the rotational degrees of freedom are discretized according to the Zwanzig model [17].

$\nu < 0$ (I stands for the isotropic phase) [14]. A schematic representation of these nematic phases is given in Fig. 1(b)-(d). The case $\nu = 0$ describes the optimal “brick” shape exactly in between “rod-like” and “plate-like”. In this case the N_U phase is suppressed and substituted by a Landau tetracritical IN_B transition [14].

The first experimental realization of the hard-cuboid model was found only recently in a colloidal suspension of boardlike mineral goethite particles [12]. By producing particles with shape parameter $\nu \simeq 0.1$ close to zero ($\langle L \rangle \times \langle W \rangle \times \langle T \rangle = 254 \times 83 \times 28 \text{ nm}^3$ and size polydispersity of 20–25%), the authors were able to produce an N_B phase stable over a pressure range surprisingly much wider than to be expected from theory [9] and simulations [15] for particles whose shape parameter deviates even slightly from zero. Even more interestingly, the authors affirm that *no* N_U phase was observed, contrasting to Ref. [14]. They suggest that a possible reason for this disagreement should be found in ingredients whose effects have never been studied so far because of their complexity, i.e. fractionation, sedimentation and polydispersity. These unexpected results motivate our interest in analyzing the effect of the above mentioned ingredients, in particular polydispersity, on the stability of the N_B phase in a fluid of hard cuboids.

We consider an M -component suspension of N_α colloidal cuboidal particles of species $\alpha = 1, \dots, M$ with dimensions $L_\alpha \times W_\alpha \times T_\alpha$ ($L_\alpha > W_\alpha > T_\alpha$) in a volume V at temperature T . The total number density of colloids is $n = \sum_\alpha N_\alpha/V$, the mole fraction of species α is $x_\alpha = N_\alpha/(nV)$ and the packing fraction is $\eta = n \sum_\alpha x_\alpha L_\alpha W_\alpha T_\alpha$. The theoretical framework used in this Letter consists of Onsager theory of liquid crystals [16]. In order to facilitate the calculations we follow Zwanzig by restricting the orientations of the particles to the six in which their principal axes are aligned along a fixed Cartesian frame [17]. Although quantitative agreement with real systems is not expected because of the simplifications introduced in the model, the same model was shown to successfully predict non-trivial phenomena like demixing in rod-plate mixtures [10], orientational wetting due to confinement and capillary nematicization [18]. Denoting the density of particles of species $\alpha = 1, \dots, M$ with orientation $i = 1, \dots, 6$ by ρ_i^α , we can write the Onsager-type free-energy functional \mathcal{F} as

$$\frac{\mathcal{F}}{V k_B T} = \sum_{\alpha=1}^M \sum_{i=1}^6 \left\{ \rho_i^\alpha [\ln(\rho_i^\alpha) - 1] + \frac{1}{2} \sum_{\alpha'=1}^M \sum_{i'=1}^6 E_{ii'}^{\alpha\alpha'} \rho_i^\alpha \rho_{i'}^{\alpha'} \right\}, \quad (2)$$

where k_B is the Boltzmann constant and $E_{ii'}^{\alpha\alpha'}$ is the excluded-volume between rods of species α and α' and orientations i and i' , respectively (see Appendix B). The equilibrium distribution ρ_i^α is the one that minimizes \mathcal{F} under the constraints that $\sum_i \rho_i^\alpha = n x_\alpha$ for all $\alpha = 1, \dots, M$.

Our analysis starts by considering the simplest case of polydispersity, i.e. a mixture of $M = 2$ components

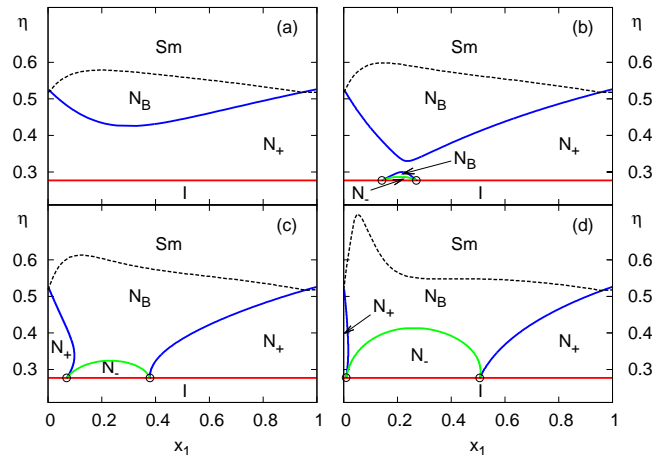


FIG. 2. (Color online) Phase diagram of a binary mixture of hard cuboids in terms of packing fraction η vs. mole fraction of the larger component x_1 showing isotropic (I), uniaxial (N_+ and N_-) and biaxial (N_B) nematic and smectic (Sm) phases. The size of the particles is defined by Eq. (3) with $L/T = 9.07$, $W/T = 2.96$ ($\nu = 0.1$) and bidispersities (a) $s = 0.15$, (b) $s = 0.18$, (c) $s = 0.20$, (d) $s = 0.30$. The solid lines separate different homogeneous phases, the dashed lines indicate the limit of stability of the homogeneous phases with respect to smectic fluctuations, whereas the open circles represent the Landau tetracritical points.

with mole fractions x_1 and $x_2 = 1 - x_1$, respectively. Among the different ways one can parameterize polydispersity, our preliminary analysis suggests to consider *volume polydispersity* (i.e. species with same particle shape but different particle volume). Therefore, we study the phase behavior of a binary mixture of hard cuboids whose dimensions are

$$\begin{aligned} L_1 &= L(1+s), & W_1 &= W(1+s), & T_1 &= T(1+s), \\ L_2 &= L(1-s), & W_2 &= W(1-s), & T_2 &= T(1-s), \end{aligned} \quad (3)$$

where the parameter $s \in [0, 1)$ describes the degree of bidispersity. Notice that Eq. (3) implies the same aspect ratios for both species $L_1/T_1 = L_2/T_2 = L/T$ and $W_1/T_1 = W_2/T_2 = W/T$ (hence $\nu_1 = \nu_2 = \nu$). Here we set $L/T = 9.07$ and $W/T = 2.96$ ($\nu = 0.1$) in order to reproduce the experimental system of Ref. [12], while neglecting the small effect of the ionic double layer used by the authors to interpret the experimental data.

Fig. 2 shows density-composition phase diagrams of binary mixtures ($M = 2$) of boardlike particles with the experimental shape parameter $\nu = 0.1$ for various bidispersity parameters (a) $s = 0.15$, (b) 0.18, (c) 0.20 and (d) 0.30, featuring isotropic (I), uniaxial nematic (N_+ and N_-), biaxial nematic (N_B) and smectic (Sm) phases. Due to the near-perfect “biaxial” shape of the particles, fractionation is extremely weak and invisible on the scale of Fig. 2 (see Appendix D). At the extreme mole fractions $x_1 = 0$ and $x_1 = 1$ (pure systems) all phase diagrams feature the phase sequence $I \rightarrow N_+ \rightarrow Sm$ that is

well known and expected for board-shaped particles with $\nu > 0$, with the N_B phase metastable with respect to the Sm phase [9, 14] (see Appendix E). However, for all s there is a composition regime in which the N_B phase is found to be stable, the more so for increasing s . Whereas the opening-up of a stable N_B regime is only quantitative for $s = 0.15$, there is a qualitative change of the phase diagram topology beyond $s = 0.18$, where *two* Landau tetracritical points appear (open circles in Figs. 2(b)-(d)). The appearance of these critical points is surprising for the rod-shaped particles ($\nu > 0$) of interest, since it coincides with a region in the phase diagram where the *oblate* uniaxial nematic N_- phase is stable rather than the expected *prolate* N_+ phase. Clearly, Figs. 2(c) and (d) show that the stability region of both N_- and N_B enlarges with increasing bidispersity. In other words, the excluded-volume interactions in mixtures of board-shaped rods tend to stabilize the N_- and N_B phases at the expense of the N_+ and the Sm phases. The reduced stability of the Sm phase is not a surprise, given that regular packing into layers is hindered by size differences between particles.

It is interesting to understand how the remarkable features of the binary mixture described in Fig. 2 change with the shape of the particles. Here we are mainly interested in two properties of the phase diagram: (i) the minimum threshold bidispersity s_{thr} at which the Landau tetracritical points appear and (ii) the tetracritical mole fractions x_1^* in terms of the bidispersity s . In Eq. (3) the shape of the particles is determined by the two aspect ratios L/T and W/T ; however, in order to visualize the deviations from the optimal “brick” shape, we use here a representation in which one of the two aspect ratios is fixed (e.g. W/T) and $\nu = L/W - W/T$ is varied by varying the remaining one (e.g. L/T). Fig. 3(a) shows for $W/T = 2.0, 2.96, 4.0$ and 5.0 a similar trend: the minimum threshold bidispersity s_{thr} increases the more the shape deviates from the optimal “brick” one. At the same time, the fact that at fixed ν the threshold bidispersity decreases with W/T , indicates that the appearance of the Landau tetracritical points is favored by an increasing aspect ratio of the particles. Interestingly, this is in agreement with the observation that shape anisotropy favors N_B stability in monodisperse hard cuboids [19]. Moreover, by fixing the aspect ratio $W/T = 2.96$, we can observe in Fig. 3(b) the tetracritical mole fraction as a function of the bidispersity for different values of $\nu = 0.01, 0.1$ and 0.25 . We note in this case that the closer the shape is to the optimal “brick”, the wider is the difference in value of the two tetracritical mole fractions x_1^* and, consequently, the stability regime of the N_- phase. Finally, we note that no critical composition is observed if the particles are closer to the “plate-like” shape, i.e. if $\nu_1 = \nu_2 = \nu < 0$ one finds the N_- in between the I and N_B phases for every value of s and x_1 (not shown); the N_+ phase does *not* occur in this case.

In order to more realistically model the experimental system of Ref. [12], we extend our phase-diagram calcu-

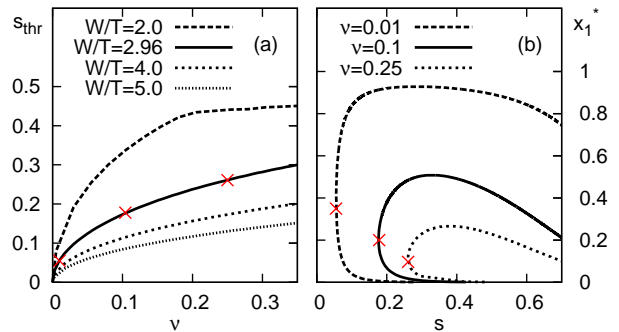


FIG. 3. (Color online) (a) Threshold bidispersity s_{thr} for the appearance of a tetracritical point as a function of the shape parameter ν for different fixed values of W/T . (b) Critical mole fraction x_1^* as a function of the bidispersity parameter s for a binary mixture of hard cuboids for different shape of the particles (cf. Eq. (3)). The red crosses, indicating the threshold bidispersity, are reported also in Fig. 3(a).

lations to a system with $M = 21$ components of cuboids. Inspired by our analysis of the binary mixture and by the experiments [12], we fix the aspect ratios of all species to $L_\alpha/T_\alpha = L/T = 9.07$ and $W_\alpha/T_\alpha = W/T = 2.96$, such that (i) all species have the same shape $\nu_\alpha = \nu = 0.1$ and (ii) the size of each species is completely determined by T_α . We consider T_α to be distributed according to a discretized Gaussian function with average $\langle T \rangle = 28$ nm and standard deviation $\sigma \langle T \rangle$, where σ is the size polydispersity. Note that σ plays the same role in the polydisperse case as s in the binary case. In general the calculation of a (high-dimensional) phase diagram of a multi-component system is a daunting task [20]. In this case, however, it is justified to ignore fractionation (see Appendix D), which reduces the problem to minimizing the functional with respect to ρ_i^α at fixed nx_α . The resulting phase diagram in the density-polydispersity representation is shown in Fig. 4(a), featuring again I, N_+, N_-, N_B and Sm equilibrium states and a tetracritical point at $\sigma \simeq 25\%$, which is surprisingly close to the size polydispersity in the experiments [12]. The strikingly large stability regime of the N_B is caused by the reduced stability of Sm and N_+ , not unlike in the binary case.

Although our results so far give strong evidence for a polydispersity-induced stability of the N_B phase in dispersions of board-shaped particles, our bulk phase diagrams cannot be compared directly with the experiments of Ref. [12], as these involve a sedimentation-diffusion equilibrium in the Earth’s gravity field. Within a local density approximation (LDA) and a Parsons-Lee correction to account for higher-order virial terms (see Appendix F), we include the effect of gravity and calculate the density profiles $\rho_i^\alpha(z)$ as a function of the height $z \in [-H, 0]$ in a dispersion column of height H and a liquid-air meniscus at $z = 0$. The phase boundaries are shown in Fig. 4(b) for the system parameters of Ref. [12], given by $\eta = 0.135$, $H = 21.5$ mm (capillary 1) and

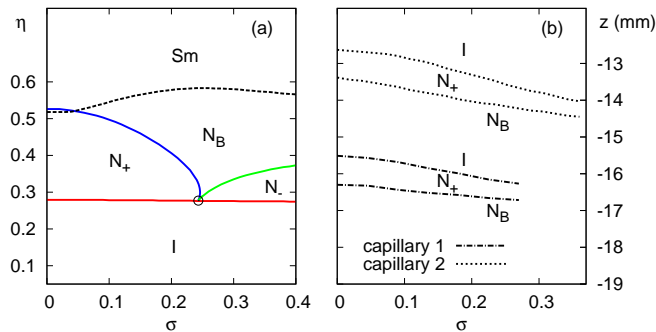


FIG. 4. (Color online) (a) Phase diagram of a system of $M = 21$ components of hard cuboids with aspect ratios $L_\alpha/T_\alpha = 9.07$ and $W_\alpha/T_\alpha = 2.96$ ($\alpha = 1, \dots, M$) and dimensions distributed according to a Gaussian function with polydispersity σ (see text). The dashed line indicates the limit of stability of the homogeneous phases with respect to smectic fluctuations, and the open circle highlights the tetracritical point. (b) Sedimentation phase diagram for the same system in terms of the standard deviation σ of the parent distribution of cuboids. The gravitational field is added into the theory within a local density approximation, and a Parsons-Lee correction reduces the effect of the second-virial truncation (see Appendix F). The average thickness $\langle T \rangle = 28$ nm and the buoyant mass density $\delta_m = 3.22$ g/ml are taken from Ref. [12], as well as the total height H and packing fraction η (capillary 1: $\eta = 0.136$, $H = 21.5$ mm; capillary 2: $\eta = 0.256$, $H = 24$ mm).

$\eta = 0.256$, $H = 24$ mm (capillary 2), as a function of the polydispersity σ of the parent distribution. Following the experiments of Ref. [12], we assume that all particles have a constant buoyant mass density ($\delta_m = 3.22$ g/ml), so that bigger particles have a higher probability to be at the bottom of the sample (see Appendix F). As a consequence, at each height z the size distribution is not Gaussian anymore, and the phase behavior deviates from that of the bulk parent distribution in a non-trivial way. Although not so manifestly as in Fig. 4(a), the range of stability of the N_+ decreases with σ also in Fig. 4(b). This suggests that sedimentation determines a displacement of the tetracritical point towards higher polydispersities. For both the capillaries, the range of stability of the N_+ phase appears to be smaller than 1 mm already at $\sigma = 0$. Given that the typical z -resolution in the experiment of Ref. [12] was of the order of 1 mm [21], the present calculations suggest that the apparent direct IN_B transition was due to the narrow stability range of the N_U phase.

In conclusion, by means of a mean-field theoretical approach with discrete orientations we have shown that size polydispersity strongly affects the phase behavior of boardlike particles, driving the emergence of a novel topology of the phase diagram. This topology change is related to the appearance of a tetracritical point, which divides the phase diagram into “rod-like”, “plate-like” and “brick-like” regions. In combination with the destabilization of the Sm phase, we can conclude that polydis-

persity dramatically increases the stability regime of the N_B phase. The usual stability limitations of N_B phases, such as demixing of rod-plate mixtures and ordering into smectics, are therefore overcome in the present model. Given the robustness of our Onsager-Zwanzig predictions with respect to the parameter choices, it may well turn out that polydispersity is also the key for N_B stability in thermotropic liquid crystals. We hope that our findings will stimulate further research in this direction.

This work is financed by a NWO-VICI grant and is part of the research program of FOM, which is financially supported by NWO.

Appendix A: Notation

k_B	Boltzmann constant
T	absolute temperature
V	volume
M	total number of species
N_α	number of particles belonging to species α
$N = \sum_\alpha N_\alpha$	total number of particles
$x_\alpha = N_\alpha/N$	mole fraction of species α
μ_α	chemical potential of species α
$n = N/V$	number density
$L_\alpha > W_\alpha > T_\alpha$	size of the principal axes of cuboids belonging to species α
$v_\alpha = L_\alpha W_\alpha T_\alpha$	particle volume of species α
$\eta = \sum_\alpha \frac{N_\alpha}{V} v_\alpha$	packing fraction

In this work Latin letters (e.g. i) indicate rotational configurations, whereas Greek letters (e.g. α) denote the chemical components of the system. To simplify the equations involved we define, unless otherwise specified,

$$\sum_i \equiv \sum_{i=1}^6, \quad \sum_\alpha \equiv \sum_{\alpha=1}^M, \quad \int d\mathbf{r} \equiv \int_V d\mathbf{r}. \quad (\text{A1})$$

According to the Zwanzig model [17] the number of independent rotational configurations of a cuboid is 6. Each configuration is defined by the direction along which the three principal axes of the cuboid L , W and T are aligned and is identified by a number $i = 1, \dots, 6$ (cf. Tab. A1).

i	L	W	T
1	x	y	z
2	z	x	y
3	y	z	x
4	x	z	y
5	y	x	z
6	z	y	x

TABLE A1. Enumeration of the rotational configurations of a hard cuboid within the Zwanzig model.

Appendix B: Density functional theory

In the density functional theory framework [22] applied to the Zwanzig model [17], the free energy \mathcal{F} of a thermodynamic system is expressed as a functional of the single-particle density $\rho_i^\alpha(\mathbf{r})$ at position $\mathbf{r} = (x, y, z)$. This functional is given by the sum of an ideal and an excess term

$$\frac{\mathcal{F}[\rho]}{k_B T} = \int d\mathbf{r} \sum_{\alpha,i} \rho_i^\alpha(\mathbf{r}) \left[\ln(\rho_i^\alpha(\mathbf{r}) \Lambda_\alpha^3) - 1 \right] + \frac{\mathcal{F}^{ex}[\rho]}{k_B T}. \quad (\text{A1})$$

In general, the excess term $\mathcal{F}^{ex}[\rho]$ has a non-trivial dependence on $\rho_i^\alpha(\mathbf{r})$. For short-range potentials it is always possible to express $\mathcal{F}^{ex}[\rho]$ as a virial series in the single-particle density, such that, at second virial order

$$\frac{\mathcal{F}^{ex}[\rho]}{k_B T} = -\frac{1}{2} \int d\mathbf{r} d\mathbf{r}' \sum_{\alpha,\alpha',i,i'} f_{ii'}^{\alpha\alpha'}(\mathbf{r} - \mathbf{r}') \rho_i^\alpha(\mathbf{r}) \rho_{i'}^{\alpha'}(\mathbf{r}'), \quad (\text{A2})$$

where the Mayer function $f_{ii'}^{\alpha\alpha'}(\mathbf{r} - \mathbf{r}')$ is defined in terms of the pairwise interaction potential $u_{ii'}^{\alpha\alpha'}(\mathbf{r} - \mathbf{r}')$ as

$$f_{ii'}^{\alpha\alpha'}(\mathbf{r}) = \exp\left[-\frac{1}{k_B T} u_{ii'}^{\alpha\alpha'}(\mathbf{r})\right] - 1. \quad (\text{A3})$$

The single-particle density $\rho_i^\alpha(\mathbf{r})$ is related to the number of particles N_α through the normalization condition

$$\int d\mathbf{r} \sum_i \rho_i^\alpha(\mathbf{r}) = N_\alpha = x_\alpha N. \quad (\text{A4})$$

For hard cuboids the interaction potential, which expresses the impenetrability of the particles, is

$$u_{ii'}^{\alpha\alpha'}(\mathbf{r}) = \begin{cases} \infty & \text{if } |x| < (X_i^\alpha + X_{i'}^{\alpha'}) \\ & \text{and } |y| < (Y_i^\alpha + Y_{i'}^{\alpha'}) \\ & \text{and } |z| < (Z_i^\alpha + Z_{i'}^{\alpha'}); \\ 0 & \text{otherwise.} \end{cases} \quad (\text{A5})$$

According to the index notation defined in Sec. ??, the 6-dimensional vectors \mathbf{X}^α , \mathbf{Y}^α and \mathbf{Z}^α of species α are given in terms of the dimension of the particles by

$$\begin{aligned} \mathbf{X}^\alpha &= \frac{1}{2}(L_\alpha, W_\alpha, T_\alpha, L_\alpha, W_\alpha, T_\alpha), \\ \mathbf{Y}^\alpha &= \frac{1}{2}(W_\alpha, T_\alpha, L_\alpha, T_\alpha, L_\alpha, W_\alpha), \\ \mathbf{Z}^\alpha &= \frac{1}{2}(T_\alpha, L_\alpha, W_\alpha, W_\alpha, T_\alpha, L_\alpha). \end{aligned} \quad (\text{A6})$$

In this work we are mainly interested in phases which are spatially homogeneous, so that positional dependences of the single-particle density can be disregarded. Therefore, Eq. (A1) becomes the Onsager-Zwanzig free energy per unit volume and unit $k_B T$

$$\frac{\mathcal{F}}{V k_B T} = \sum_{\alpha,i} \rho_i^\alpha \left[\ln(\rho_i^\alpha \Lambda_\alpha^3) - 1 \right] + \frac{1}{2} \sum_{\alpha,\alpha',i,i'} E_{ii'}^{\alpha\alpha'} \rho_i^\alpha \rho_{i'}^{\alpha'}. \quad (\text{A7})$$

The thermal wavelength Λ_α does not influence the equilibrium structure, so that we set it for convenience to unity. The single-particle density is normalized according to

$$\sum_i \rho_i^\alpha = x_\alpha n. \quad (\text{A8})$$

The excluded volume $E_{ii'}^{\alpha\alpha'}$ between two particles belonging to species α and α' with orientations i and i' interacting through the potential Eq. (A5) is

$$E_{ii'}^{\alpha\alpha'} = (X_i^\alpha + X_{i'}^{\alpha'})(Y_i^\alpha + Y_{i'}^{\alpha'})(Z_i^\alpha + Z_{i'}^{\alpha'}). \quad (\text{A9})$$

Appendix C: Monodisperse system of hard cuboids

The main goal of the present work is to investigate how polydispersity affects the phase behavior, and in particular the stability of the N_B phase, in a system of hard cuboids. For this reason, it is instructive to study what the theoretical framework described in Sec. B predicts in the monodisperse case $M = 1$. In particular, we will focus here on the role of the particles dimensions on the phase behavior of the system.

In Fig. A5 we report the phase diagram of a monodisperse system of hard cuboids as a function of the aspect ratio W/T at fixed $L/T = 9.07$. Consequently, by varying W/T one varies the shape parameter $\nu = L/W - W/T$, in such a way that by crossing the point $\nu = 0$ one expects a transition from plate- to rod-like behavior. This is precisely what Fig. A5 shows, where the phase separation lines are calculated by minimizing the Onsager-Zwanzig functional Eq. (A7) with the constraint of Eq. (A8) for each value of the packing fraction η . Moreover, bifurcation theory (cf. Sec. E) provides a way to estimate the upper limit of stability of homogeneous phases with respect to the smectic (dashed line

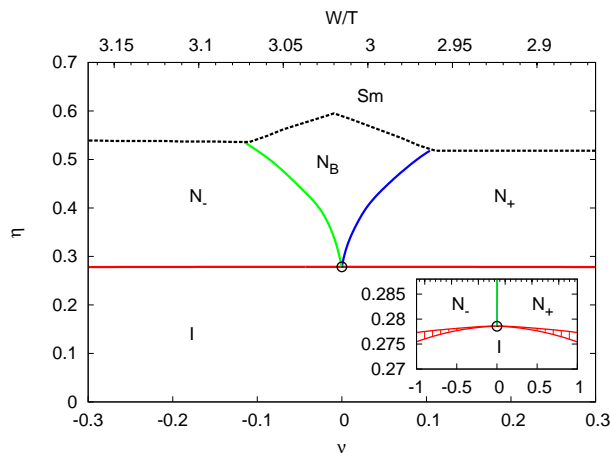


FIG. A5. Phase diagram of a monodisperse system of hard cuboids as a function of the shape parameter $\nu = L/W - W/T$ (with $L/T = 9.07$ fixed and W/T variable). The solid lines indicate phase boundaries as calculated by minimizing the Onsager-Zwanzig functional, the dashed line indicates the limit of stability of the nematic with respect to the smectic phase and the open circle the Landau tetracritical point. The inset highlights the first order character of the IN_U transition and how this tends to become continuous by approaching $\nu = 0$.

in Fig. A5). Fig. A5 shows that to observe a stable N_B phase, the shape of the particles should be designed with extremely high precision in a small ν -regime about $\nu = 0$. In fact, for $L = 9.07T$ the N_B phase disappears unless $2.96T < W < 3.08T$. This is due both to the tight cusp-like shape of the $N_U N_B$ transition line and to the preempting character of inhomogeneous phases. Analogous results can be obtained by varying the shape parameter through L/T , while keeping W/T fixed. Finally, in the inset of Fig. A5 (note the different scale) we show the first order character of the IN_U transition, which tends to become second-order by approaching the critical point at $\nu = 0$.

For the sake of completeness, in Fig. A6 we report the orientation distribution function p_i , which is the probability of a given orientation $i = 1, \dots, 6$ as a function of the packing fraction η for different values of the shape parameter ν . In the monodisperse case this function coincides with the single-particle density divided by the number density: $p_i = \rho_i/n$. The value the orientation distribution function assumes tells us about the symmetry of the corresponding phase. In fact, at a given packing fraction η in Fig. A6 one can have one of the following possibilities:

- the probabilities p_i are all the same, i.e. $p_i = 1/6$ (isotropic I phase);
- the probabilities p_i are coupled two-by-two, demonstrating the presence of a symmetry axis (uniaxial nematic N_U phase);
- the probabilities p_i are different between each oth-

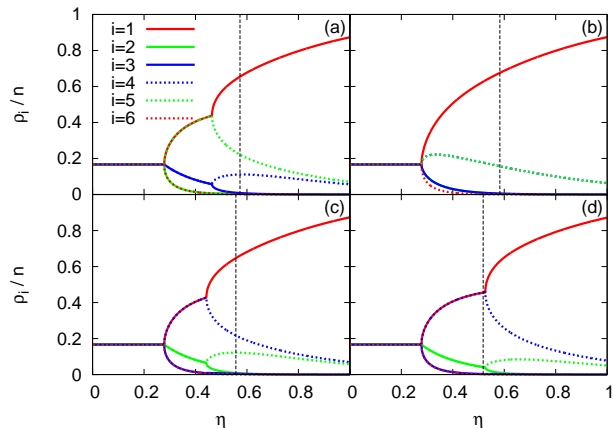


FIG. A6. Orientation distribution function of a monodisperse system of hard cuboids as a function of the packing fraction η obtained by minimization of the Onsager-Zwanzig functional Eq. (A7) for $M = 1$. The cuboids have dimensions $L/T = 9.07$ and (a) $W/T = 3.04$, (b) $W/T = 3.01$, (c) $W/T = 2.99$, (d) $W/T = 2.96$. The different lines indicate the probability of a particular orientation $i = 1, \dots, 6$ (cf. Tab. A1). The dashed vertical line shows the limit of stability of the nematic phases with respect to the smectic.

ers (biaxial nematic N_B phase).

Moreover, in the uniaxial nematic case one can further distinguish two situations:

- ▲ the two more probable orientations have the shortest axis aligned along the same direction (uniaxial nematic oblate N_- phase);
- ▲ the two more probable orientations have the longest axis aligned along the same direction (uniaxial nematic prolate N_+ phase).

This classification is easily generalized to the multi-component case. With this in mind, one can observe the difference in the orientation distribution function when $\nu = -0.06 < 0$ ($W/T = 3.04$, Fig. A6(a)), $\nu = 0$ ($W/T = 3.01$, Fig. A6(b)) and $\nu = 0.04 > 0$ ($W/T = 2.99$, Fig. A6(c)). The vertical dashed line indicates the limit of stability with respect to smectic fluctuations as given by bifurcation theory. Finally, Fig. A6(d) shows the predicted orientation distribution function when the experimental value $W/T = 2.96$ is considered [12], and highlights how according to the model the N_B phase is expected to be preempted by inhomogeneous phases.

Appendix D: Nearly second-order character of the IN_{\pm} transition

An important point addressed in the Letter is the nearly second-order character of all the phase transitions

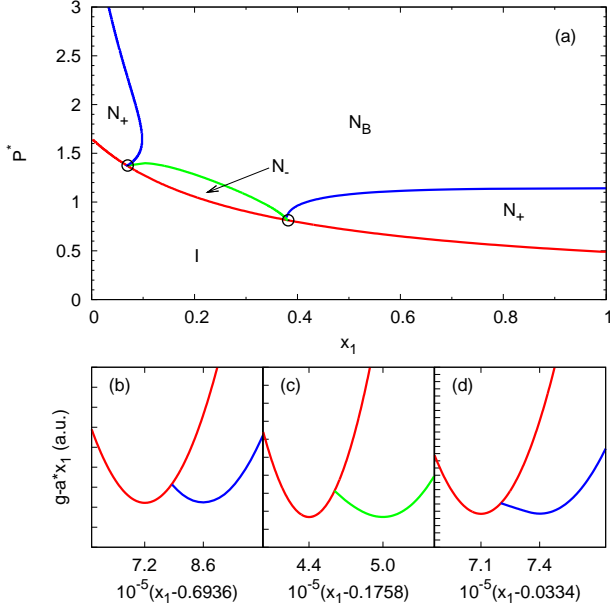


FIG. A7. (a) Phase diagram of a binary mixture of hard cuboids in terms of the reduced osmotic pressure $P^* = PLWT/(k_B T)$ vs. mole fraction of the first species x_1 . (b)-(d) I (red line), N_+ (blue line) and N_- (green line) branches of the Gibbs free energy per particle $g = G/N$ at (b) $P^* = 0.6$, (c) $P^* = 1.1$ and (d) $P^* = 1.5$. A straight line with slope $a = \partial g / \partial x_1|_{x_1=x_I} = \partial g / \partial x_1|_{x_1=x_N}$ (with x_I and x_N the compositions of the coexisting isotropic and nematic phases) was subtracted in each case to enhance the visualization of the common tangent construction.

involved in the phase diagram of volume polydisperse cuboids (cf. Fig. 2 and 4(a)). In particular, although Landau-de Gennes theory predicts the IN_U transition to be first order [23], we will show here that in the binary mixture defined by Eq. (4) its discontinuous character can be neglected at any mole fraction x_1 . Consequently, we can suppose that the same holds for an arbitrary number of components as a consequence of the almost second-order character of the transition in the monodisperse case (cf. inset of Fig. A5). There is no simple way to demonstrate the validity of this assumption, but we take it for granted because of the simplifications it brings in the calculation of the phase diagram for $M > 2$.

When dealing with mixtures, the phase diagram is conveniently expressed in terms of the osmotic pressure P vs. the mole fraction x_α of $M - 1$ components. In this way it is possible to visualize the coexistence of phases characterized by a different composition with respect to the parent distribution. This phenomenon, called demixing or fractionation, is a consequence of the first-order character of the phase transition involved. Here we analyze demixing in a binary mixture of cuboids parameterized as in Eq. (4) with $L/T = 9.07$, $W/T = 2.96$ and $s = 0.2$. In Fig. A7(a) we report the phase diagram for such a system as a function of the mole fraction x_1

of the larger species. At three different values of the reduced pressure $P^* = PLWT/(k_B T)$ we calculated the isotropic and uniaxial nematic branches of the relevant thermodynamic potential, i.e. the Gibbs free energy per particle $g(P, x_1) = G(P, N_1, N_2)/(N_1 + N_2)$. The coexistence between the two phases is given by a common tangent construction, which allows to evaluate the difference in composition Δx_1 of the coexisting phases. The results are reported in Fig. A7(b)-(d) for $P^* = 0.6, 1.1$ and 1.5 respectively. In the three cases, two of which describe a IN_+ and one a IN_- transition, $\Delta x_1 \approx 10^{-5}$ and can therefore be neglected. The situation does not change when one considers different values of the bidispersity parameter s .

Appendix E: Nematic-Smectic bifurcation

Bifurcation theory [24, 25] provides a way to investigate the limit of stability of a particular phase. The condition of thermodynamic stability of a phase described by the single-particle density $\rho_i^\alpha(\mathbf{r})$ requires that the system corresponds to a minimum of the free energy \mathcal{F} , i.e. a stationary point that satisfies

$$\int d\mathbf{r} d\mathbf{r}' \sum_{\alpha, \alpha', i, i'} \frac{\delta^2 \mathcal{F}}{\delta \rho_i^\alpha(\mathbf{r}) \delta \rho_{i'}^{\alpha'}(\mathbf{r}')} \delta \rho_i^\alpha(\mathbf{r}) \delta \rho_{i'}^{\alpha'}(\mathbf{r}') > 0, \quad (\text{A1})$$

for any arbitrary perturbation $\delta \rho_i^\alpha(\mathbf{r})$. By inserting the functional expression Eq. (A1) into Eq. (??), one finds that the reference phase (described by $\rho_i^\alpha(\mathbf{r})$) ceases to be stable at the smallest density $n = N/V$ at which a perturbation $\delta \rho_i^\alpha(\mathbf{r})$ exists such that

$$\delta \rho_i^\alpha(\mathbf{r}) = \rho_i^\alpha(\mathbf{r}) \int d\mathbf{r}' \sum_{\alpha', i'} f_{ii'}^{\alpha\alpha'}(\mathbf{r} - \mathbf{r}') \delta \rho_{i'}^{\alpha'}(\mathbf{r}'). \quad (\text{A2})$$

We are interested in calculating the limit of stability of the (uniaxial or biaxial) nematic phase with respect to smectic fluctuations. With this in mind, in Eq. (A2) we impose no positional dependence on the reference phase, i.e. $\rho_i^\alpha(\mathbf{r}) = \rho_i^\alpha$, and a positional dependence of the fluctuations only along the z direction, i.e. $\delta \rho_i^\alpha(\mathbf{r}) = \delta \rho_i^\alpha(z)$. After some rearranging Eq. (A2) becomes

$$\sigma_i^\alpha(z) = \sum_{\alpha', i'} \int dz' Q_{ii'}^{\alpha\alpha'}(z - z') \sigma_{i'}^{\alpha'}(z'), \quad (\text{A3})$$

where $\sigma_i^\alpha(z) = \delta \rho_i^\alpha(z) / \sqrt{\rho_i^\alpha}$ and

$$Q_{ii'}^{\alpha\alpha'}(z) = \sqrt{\rho_i^\alpha \rho_{i'}^{\alpha'}} \int dx dy f_{ii'}^{\alpha\alpha'}(\mathbf{r}), \quad (\text{A4})$$

a symmetric (Hermitian) kernel. By inserting in Eq. (A4) the explicit form of the inter-particle potential Eq. (A5), we obtain

$$Q_{ii'}^{\alpha\alpha'}(z) = \begin{cases} -W_{ii'}^{\alpha\alpha'} & \text{if } |z| < (Z_i^\alpha + Z_{i'}^{\alpha'}) \\ 0 & \text{otherwise,} \end{cases} \quad (\text{A5})$$

where $W_{ii'}^{\alpha\alpha'} = \sqrt{\rho_i^\alpha \rho_{i'}^{\alpha'}} (X_i^\alpha + X_{i'}^{\alpha'}) (Y_i^\alpha + Y_{i'}^{\alpha'})$.

Eq. (A3) is easily solved in Fourier space, where it becomes

$$\hat{\sigma}_i^\alpha(q) = \sum_{\alpha', i'} \hat{Q}_{ii'}^{\alpha\alpha'}(q) \hat{\sigma}_{i'}^{\alpha'}(q), \quad (\text{A6})$$

with

$$\hat{Q}_{ii'}^{\alpha\alpha'}(q) = -2\sqrt{\rho_i^\alpha \rho_{i'}^{\alpha'}} E_{ii'}^{\alpha\alpha'} j_0(q(Z_i^\alpha + Z_{i'}^{\alpha'})), \quad (\text{A7})$$

and $j_0(x) = \sin(x)/x$.

In conclusion, the limit of stability of the nematic phase with respect to smectic fluctuations is given by the minimum packing fraction η^* at which there exists a wave vector q^* such that the $6M \times 6M$ matrix with entries $\hat{Q}_{ii'}^{\alpha\alpha'}(q^*)$ has a unitary eigenvalue. The periodicity of the corresponding bifurcating smectic phase is given by $\lambda^* = 2\pi/q^*$.

Appendix F: Sedimentation profiles

In the presence of gravity a particle of species α of a colloidal suspension is subject to the external potential

$$U_\alpha(z) = v_\alpha \delta_m g z, \quad (\text{A1})$$

where z is the coordinate relative to the vertical axis, g the gravitational acceleration, $v_\alpha = L_\alpha W_\alpha T_\alpha$ the particle volume and δ_m the buoyant mass density.

The external field determines an explicit breaking of the translational symmetry, which results in a single-particle density $\rho_i^\alpha(z)$ dependent on z . The single-particle density is normalized according to

$$\int_{-H}^0 dz \sum_i \rho_i^\alpha(z) = \frac{N_\alpha}{A} = \frac{x_\alpha H \eta}{\sum_{\alpha'} x_{\alpha'} v_{\alpha'}}, \quad (\text{A2})$$

where H is the total height of the sample, A its transverse area and η the overall packing fraction. In terms of the single-particle density $\rho_i^\alpha(z)$ and the chemical potentials $\{\mu_\alpha\}$, the grand-potential functional Ω is [22]

$$\Omega[\rho_i^\alpha(z)] = \mathcal{F}^{id} + \mathcal{F}^{ex} - A \int dz \sum_{\alpha, i} [\mu_\alpha - U_\alpha(z)] \rho_i^\alpha(z), \quad (\text{A3})$$

where \mathcal{F}^{id} is the ideal contribution to the intrinsic free energy

$$\frac{\mathcal{F}^{id}[\rho_i^\alpha(z)]}{k_B T} = A \int_{-H}^0 dz \sum_{\alpha, i} \rho_i^\alpha(z) \{\log[\rho_i^\alpha(z)] - 1\}, \quad (\text{A4})$$

whereas \mathcal{F}^{ex} the excess one. In the case it is legitimate to assume that the single-particle density varies slowly on the scale of the particle dimensions, introducing a local density approximation allows to simplify the excess term in the intrinsic free energy as follows [26]

$$\frac{\mathcal{F}^{ex}[\rho_i^\alpha(z)]}{k_B T} = \frac{A}{2} \int_{-H}^0 dz G[\rho_i^\alpha(z)] \sum_{\alpha, \alpha', i, i'} E_{ii'}^{\alpha\alpha'} \rho_\alpha^i(z) \rho_{\alpha'}^{i'}(z). \quad (\text{A5})$$

The Parsons-Lee factor $G[\rho_i^\alpha(z)]$ is introduced in order to reduce the effect of the truncation due to the second-virial approximation [27]. By introducing the local packing fraction

$$\eta(z) = \sum_{\alpha, i} \rho_i^\alpha(z) v_\alpha, \quad (\text{A6})$$

the Parsons-Lee factor can be written as

$$G[\rho_i^\alpha(z)] = \frac{4 - 3\eta(z)}{4(1 - \eta(z))^2}. \quad (\text{A7})$$

The second-virial approximation can be recovered by setting $G[\rho_i^\alpha(z)] = 1$. The equilibrium single-particle density is obtained by minimizing Eq. (A3) with the constraints of Eqs. (A2) for every species α .

As an example, in what follows we address in some detail the problem of calculating the sedimentation profile for a monodisperse system of hard cuboids. The polydisperse case, although mathematically more involved and computationally more demanding, is analogous. We refer to the experiment of Ref. [12] for the values of the input parameters, so that here the dimensions of the particles are $L \times W \times T = 284 \times 83 \times 28 \text{ nm}^3$ and the buoyant mass density is $\delta_m = 3.22 \text{ g/ml}$. The height of the sample and its total packing fraction are taken in order to reproduce capillary 2 of Ref. [12], so that $H = 24 \text{ mm}$ and $\eta = 0.256$.

In Fig. A8 we report the orientation distribution function ((a) and (b)) and the packing fraction profile ((c) and (d)) for the system considered. In particular, we compare here the results obtained with ((b)-(d)) and without ((a)-(c)) the Parsons-Lee approximation. In both cases by moving towards the bottom of the sample one observes a $I \rightarrow N_+ \rightarrow N_B$ sequence of homogeneous phases, while we do not consider here inhomogeneous ones. The range of stability in height of the N_+ phase is $\Delta z_{N_+} \simeq 1 \text{ mm}$. By comparing the two sets of results one can observe how the second-virial approximation underestimates the osmotic pressure, leading to unphysical values of the packing fraction exceeding unity (cf. Fig. A8(c)). As a result,

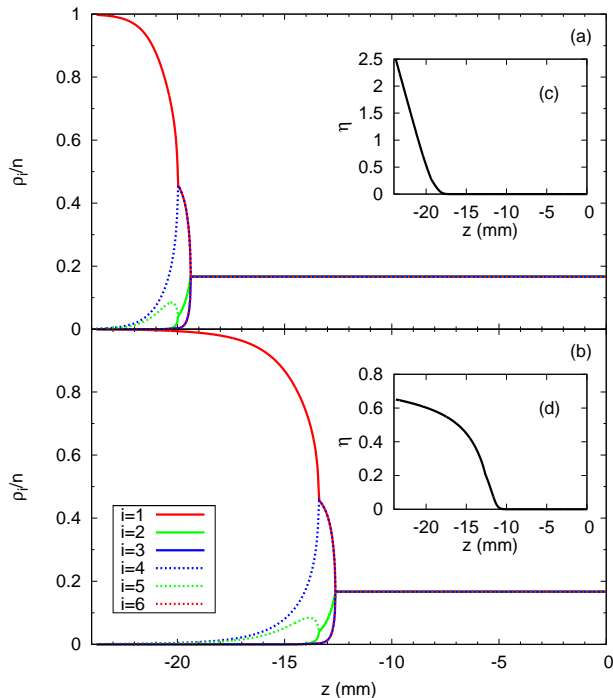


FIG. A8. (a)-(b) Orientation distribution function of a monodisperse system of hard cuboids with dimensions $L \times W \times T = 284 \times 83 \times 28$ nm and buoyant mass density $\delta_m = 3.22$ g/ml in a sample of height $H = 24$ mm at a total packing fraction $\eta = 0.256$ (a) without and (b) with Parsons-Lee approximation. (c)-(d) Corresponding packing fraction profiles (c) without and (d) with Parsons-Lee approximation.

the isotropic-nematic phase transition is shifted towards the bottom of the sample at $z_{IN} \simeq -20$ mm, whereas in the experiment $z_{IN} \simeq -4$ mm [12]. The Parsons-Lee approximation prevents the packing fraction to take non-physical values (cf. Fig. A8(d)) and shifts the IN transition to the more realistic $z_{IN} \simeq -13$ mm. However, the deviation of z_{IN} with the experimental value suggests that the Parsons-Lee correction alone does not provide quantitative agreement, and other approximations like restricting the orientations or neglecting inhomogeneous phases can play a role in this case. In conclusion, the theoretical framework developed here does not allow for quantitative agreement with the experiment. Nonetheless, the qualitative conclusion we can draw is that sedimentation determines a profile of phases in which the nematic uniaxial N_+ occupies only a narrow range in height.

-
- [1] M. J. Freiser, Phys. Rev. Lett. **24**, 1041 (1970).
[2] R. Alben, Phys. Rev. Lett. **30**, 778 (1973).
[3] J. P. Straley, Phys. Rev. A **10**, 1881 (1974).
[4] C. Tschierske and D. J. Photinos, J. Mater. Chem. **20**, 4263 (2010); R. Berardi *et al.*, J. Phys.: Condens. Matter **20**, 463101 (2008).
[5] R. Berardi, L. Muccioli and C. Zannoni, J. Chem. Phys. **128**, 024905 (2008).
[6] G. R. Luckhurst, Nature **430**, 413 (2004).
[7] L. J. Yu and A. Saupe, Phys. Rev. Lett. **45**, 1000 (1980).
[8] L. A. Madsen *et al.*, Phys. Rev. Lett. **92**, 145505 (2004); B. R. Acharya, A. Primak and S. Kumar, Phys. Rev. Lett. **92**, 145506 (2004).
[9] M. P. Taylor and J. Herzfeld, Phys. Rev. A **44**, 3742 (1991).
[10] R. van Roij and B. Mulder, J. Phys. (France) II **4**, 1763 (1994).
[11] F. M. van der Kooij and H. N. W. Lekkerkerker, Phys. Rev. Lett. **84**, 781 (2000).
[12] E. van den Pol *et al.*, Phys. Rev. Lett. **103**, 258301 (2009).
[13] G. J. Vroege and H. N. W. Lekkerkerker, J. Phys. Chem. **97**, 3601 (1993).
[14] B. Mulder, Phys. Rev. A **39**, 360 (1989).
[15] P. J. Camp and M. P. Allen, J. Chem. Phys. **106**, 6681 (1997).
[16] L. Onsager, Ann. N.Y. Acad. Sci. **51**, 627 (1949).
[17] R. Zwanzig, J. Chem. Phys. **39**, 1714 (1963).
[18] R. van Roij, M. Dijkstra and R. Evans, Europhys. Lett. **43**, 350 (2000).
[19] Y. Martínez-Ratón, S. Varga and E. Velasco, arXiv: 1103.0391 (2011).
[20] P. Sollich and M. E. Cates, Phys. Rev. Lett **80**, 1365 (1998); P. B. Warren, Phys. Rev. Lett. **80**, 1369 (1998); N. Clarke *et al.*, J. Chem. Phys. **113**, 5817 (2000).
[21] G. J. Vroege, private communication.
[22] R. Evans, Adv. Phys. **28**, 143 (1979).
[23] P. G. de Gennes and J. Prost, *The Physics of Liquid Crystals* (Clarendon, Oxford, 1993).
[24] R. F. Kaiser and H. J. Raveché, Phys. Rev. A **17**, 2067 (1978).
[25] B. Mulder, Phys. Rev. A **35**, 3095 (1987).
[26] R. Allen, D. Goulding and J.P. Hansen, Phys. Chem. Comm. **7**, 30 (1999).
[27] J. D. Parsons, Phys. Rev. A **19**, 1225 (1979); S. D. Lee, J. Chem. Phys. **87**, 4972 (1987); S. D. Lee, J. Chem. Phys. **89**, 7036 (1988).